NANO LETTERS

pubs.acs.org/NanoLett Letter

Spatial Coherence Manipulation on the Disorder-Engineered Statistical Photonic Platform

Leixin Liu, Wenwei Liu,* Fei Wang, Hua Cheng,* Duk-Yong Choi, Jianguo Tian, Yangjian Cai,* and Shuqi Chen*

Cite This: *Nano Lett.* 2022, 22, 6342−6349 Read Online

ACCESS | Metrics & More | Article Recommendations | Supporting Information

ABSTRACT: Coherence, similar to amplitude, polarization, and phase, is a fundamental characteristic of the light fields and is dominated by the statistical optical property. Although spatial coherence is one of the pivotal optical dimensions, it has not been significantly manipulated on the photonic platform. Here, we theoretically and experimentally manipulate the spatial coherence of light fields by loading different random phase distributions onto the wavefront with a metasurface. We achieve the generation of partially coherent light with a predefined degree of coherence and continuously modulate it from coherent to incoherent by controlling the phase fluctuation ranges or the beam sizes. This design strategy can be easily extended to manipulate arbitrary phase-only special beams with the same degree of coherence. Our approach provides straightforward rules to manipulate the coherence of light fields in an extra-cavity-based manner and paves the way for further applications in ghost imaging and information transmission in turbulent media.

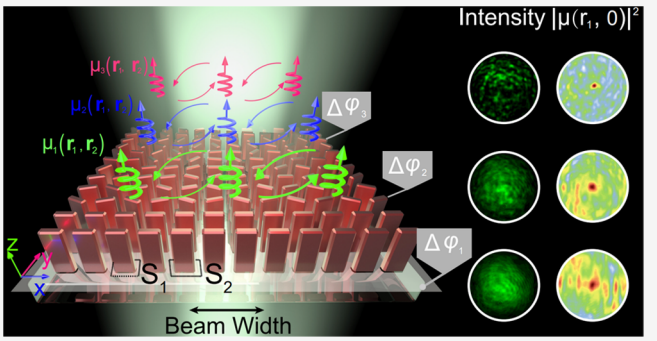

KEYWORDS: *Coherence, light manipulation, statistical metasurface*

Coherence as a second-order statistical effect is one of the most important concepts in optics and is related to the ability of light to exhibit interference effects. The coherence of electromagnetic waves (EMWs) is determined by the statistical optical property and the phase space occupation of photons,[1,2] which has boosted the development of lasers, precision measurements, and information transmission. By generating light beams with reduced coherence, i.e., partially coherent beams, one can realize numerous applications such as plasma-instability suppression,[3] ghost imaging,[4] holographic artifact suppression,[5] and optical communication, which can significantly reduce the scintillation and beam wandering caused by turbulent optical media.[6] Generally, the coherence manipulation is based on incoherent superposition of different optical modes, such as the Hermite-Gaussian modes and Laguerre-Gaussian modes, the modes with random fluctuations of amplitude and phase.[7−11] One of the most effective strategies to generate partially coherent beams is intra-cavity-based. Direct and efficient manipulation of the spatial coherence in a laser cavity can be achieved by controlling the number of transverse lasing modes,[12] generating different spatial lasing modes with different emission profiles[13] or disrupting the formation of lasing modes.[14] The aforementioned methods can be applied to suppress the laser speckles by adopting an intracavity diffuser.[15] Recently, Koivurova et al. theoretically proved the realization of polarized coherence switching[16] by incorporating an epsilon-near-zero metamaterial layer as one of the reflectors in a laser cavity, which opened up the possibility of realizing coherence-manipulation-based applications with metamaterials.

An extra-cavity-based strategy to modulate the coherence can easily satisfy the requirements of different types of incident beams and emergent light beams, thus resulting in increased compatibility and enabling a high degree of freedom to manipulate the optical fields. However, the extra-cavity-based generation of partially coherent beams traditionally requires a combination of various optical components such as lenses, rotating ground glass, and a spatial light modulator with specific distances between them.[17] This process is complex, bulky, and challenging to execute on a single photonic platform. Besides, the accurate manipulation of the degree of coherence (DOC) is limited due to the inevitable statistical roughness of the ground glass or other disordered media. In the past decade, metasurfaces have attracted increasing attention due to their great potential in integrated optical systems and advanced photonics. Metasurfaces exploit the abundant local electromagnetic resonances of

Received: May 25, 2022
Revised: July 20, 2022
Published: July 25, 2022

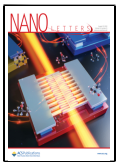

https://doi.org/10.1021/acs.nanolett.2c02115
Nano Lett. 2022, 22, 6342−6349

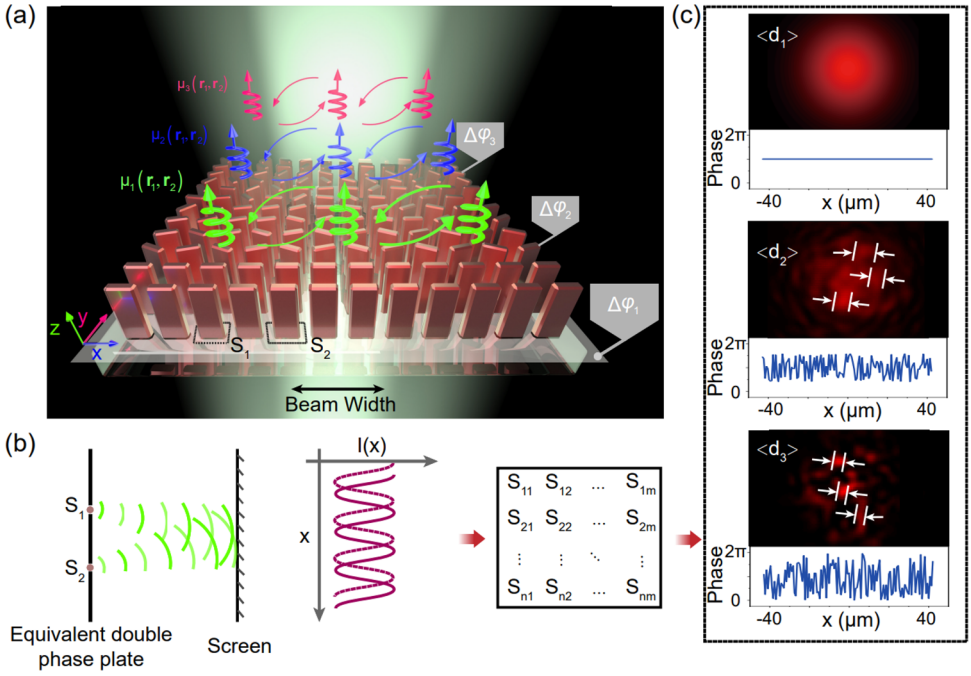

Figure 1. Design of the statistical metasurface and its operation principle. (a) Schematic of the statistical metasurface that can generate light beams with different degrees of spatial coherence. (b) Diagram of the coherence of a wave generated by any two points on the statistical metasurface. Different equivalent phase plates form phase arrays with different statistical properties. (c) Theoretical intensity distributions of light speckles (top) generated by different phase distributions (bottom). The smaller the size <*d*> of the speckle, the lower the spatial coherence of the transmitted beam.

meta-atoms and can thus provide strong light-matter interactions on the subwavelength scale with high efficiency, such as electromagnetic multipole generation,[18,19] Fano resonances,[20] bound states in the continuum,[21] and nonlinear generation.[22] Such resonances locally introduce abrupt wavefront changes in an ultrathin plane, leading to significant wavefront[23,24] and polarization[25−27] manipulation of EMWs. Although several optical dimensional manipulations such as amplitude, polarization, and phase of EMWs[28−31] have been systematically investigated, the spatial coherence as another pivotal optical dimension has not been significantly manipulated on the extra-cavity-based photonic platform. Li et al. proposed that the spatial coherence can be manipulated through surface plasmon polaritons[32] that provide a near-field-based strategy for coherence manipulation on the subwavelength scale. However, the wide range of statistical optical properties and their applications, especially their compatibility with different light beams on the photonic platform, are yet to be revealed.

In this paper, we introduce an extra-cavity-based strategy with disorder-engineered statistical metasurfaces to accurately manipulate the spatial coherence of EMWs by projecting different random phase distributions onto the wavefront or modulating the beam sizes. The statistical photonic properties such as information entropy are quantitatively investigated, and the experimental results are consistent with the theoretical predictions. The proposed strategy can also be easily extended to manipulate the spatial coherence of different special beams such as a partially coherent vortex beam with the same DOC. This approach paves the way for a new direction in statistical photonic manipulation and provides a gateway to apply partially coherent beams in informational photonic systems.

Concept of the disorder-engineered statistical metasurface. To quantify the statistical properties on the photonic platform, we begin with defining the harmonic formula of the electric fields of EMWs

$$E(\mathbf{r}, t) = A(\mathbf{r})\exp[i\varphi(\mathbf{r}, t)] \tag{1}$$

where $A(\mathbf{r})$ and $\varphi(\mathbf{r}, t)$ denote the amplitude and phase of the electric fields at an arbitrary point $\mathbf{r}$. Generally, the statistical behavior of $\varphi(\mathbf{r}, t)$ decides the coherence of the EMWs that can be described by the mutual coherence function (MCF) in the space-time domain[33]

$$\Gamma(\mathbf{r}_1, \mathbf{r}_2, \tau) = \langle E(\mathbf{r}_1, t_1)E^*(\mathbf{r}_2, t_2)\rangle \tag{2}$$

where $\tau = t_2 - t_1$, the asterisk denotes the complex conjugate, and the angle brackets denote an ensemble average over the fluctuating fields. By combining eqs 1 and 2, the MCF can be expressed as

$$\Gamma(\mathbf{r}_1, \mathbf{r}_2, \tau) = A(\mathbf{r}_1)A^*(\mathbf{r}_2)\langle\exp[i\varphi(\mathbf{r}_1, t_1) - i\varphi^*(\mathbf{r}_2, t_2)]\rangle \tag{3}$$

where we assume that $A(\mathbf{r})$ does not change with $\mathbf{r}$ for convenience. For narrowband or quasimonochromatic EMWs, the longitudinal coherence length of light is much greater than the maximum path-length difference between $\mathbf{r}_1$ and $\mathbf{r}_2$. Thus, the MCF is a slowly varying function in the τ domain and can be simplified to a mutual intensity function (MIF) $\Gamma(\mathbf{r}_1, \mathbf{r}_2) = \Gamma(\mathbf{r}_1, \mathbf{r}_2, \tau = 0)$. Accordingly, the DOC of a scalar partially coherent beam can be expressed as

$$\mu(\mathbf{r}_1, \mathbf{r}_2) = \frac{\Gamma(\mathbf{r}_1, \mathbf{r}_2, \tau = 0)}{\sqrt{\Gamma(\mathbf{r}_1, \mathbf{r}_1)\Gamma(\mathbf{r}_2, \mathbf{r}_2)}} \tag{4}$$

By substituting eq 3 in eq 4, we obtain the correlation at two arbitrary points

$$\mu(\mathbf{r}_1, \mathbf{r}_2) = \langle\exp[i\varphi(\mathbf{r}_1) - i\varphi^*(\mathbf{r}_2)]\rangle \tag{5}$$

The coherence of a beam is essentially phase-dependent, which means that the coherence of a beam can be changed by imposing different local phase fluctuations upon the EMWs. The

https://doi.org/10.1021/acs.nanolett.2c02115
Nano Lett. 2022, 22, 6342−6349

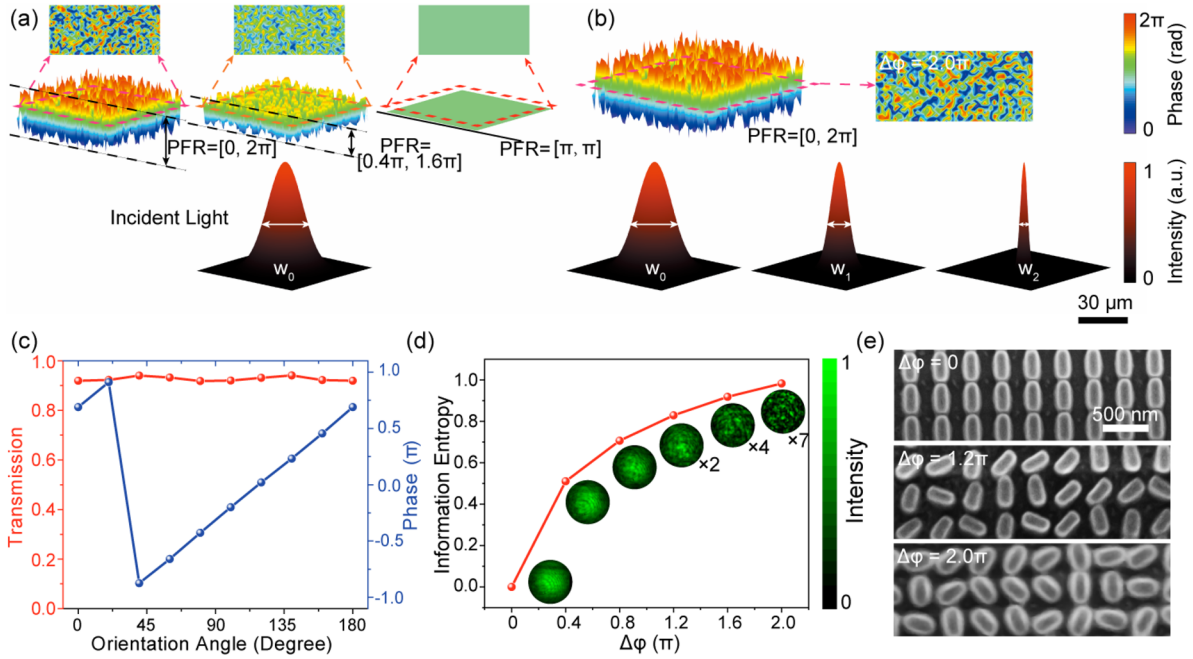

Figure 2. Design and fabrication of the dielectric nanofin array. (a) Coherence manipulation by controlling PFRs with a fixed beamwidth w_0. (b) Coherence being continuously manipulated by controlling the beamwidths with a fixed PFR. (c) Simulated cross-polarization transmission and abrupt phase change as a function of different orientation angles of the nanofins at an operating wavelength of 532 nm. (d) Calculated information entropy of the phased arrays and the instantaneous intensity of the transmitted light in each region. The intensities are normalized with the amendment coefficient on the bottom of the speckle intensity insets in (d). (e) Scanning electron microscopy (SEM) images of the fabricated metasurfaces for three different $\Delta\varphi$.

phase fluctuation of $\varphi(\mathbf{r})$ can be arbitrarily designed, and therefore, a wide range of partially coherent beams with various types of coherence functions can be realized. The schematic of the coherence-manipulated design is shown in Figure 1a. Each unit cell S_i of the sample is regarded as a phase plate, and the coherence properties of the phased array are decided by the interferences between every two plates (Figure 1b).[34] The statistical fluctuations of the transmitted fields arise due to the randomly arranged nanostructures of the phased array. Theoretically, the instantaneous light intensity of the beam generated by the statistical metasurface is Gaussian-enveloped with speckles as shown in Figure 1c, and the size of speckle <d> is related to the coherence length of the transmitted beam. By performing spatial scanning of the statistical metasurface, the wavefront of the output EMWs is spatially modulated, which statistically results in a specific DOC of the beam.

Implementation of the statistical metasurfaces with uniformly disordered phase fluctuation. The spatial coherence can be manipulated either by employing different phase fluctuation ranges (PFRs) or by varying the beam sizes with a constant PFR. A proof-of-concept design to demonstrate the proposed strategy is shown in Figure 2. To obtain the statistical properties of the metasurface, we introduce a disorder-manipulated phase distribution, with the phase of the statistical metasurface randomly and uniformly covering the PFR of $[\pi - i\pi, \pi + i\pi]$, where $i \in [0, 1]$ is a parameter for the phase design (Figure 2a). It should be noted that the phase distribution in the proposed approach is not unique. This is because the coherence of the beam is determined by the statistical generation of the optical fields. The coherence of the beam can be manipulated when the phase distribution follows the same random function. In particular, the statistical metasurface serves as a uniform phase-distributed plate when $i = 0$, i.e., $\Delta\varphi = 0$, and a perfect coherent Gaussian beam is transmitted without intensity speckles. Meanwhile, $i = 1$ indicates that the statistical metasurface is completely phase-disordered as $\Delta\varphi = 2\pi$, resulting in nearly incoherent transmitted light. The coherence length is determined by the amounts of phase fluctuations occurring in the wavefront. Thus, the coherence of the output light can also be continuously manipulated by controlling the beam sizes (Figure 2b). The building blocks of the disorder-engineered statistical metasurface are TiO_2 nanofins with a length of 260 nm, a width of 90 nm, and a height of 550 nm. The lattice size of the statistical metasurface is 330 nm. The transmitted phase can be locally manipulated following the P−B phase formula $\varphi(\mathbf{r}) = 2\sigma\theta(\mathbf{r})$, where $\sigma = \pm 1$ represents the left-/right-handed circularly polarized incident light, φ is the cross-polarized transmitted phase, and θ is the local orientation angle of the nanofin (Figure 2c). Such large-aspect-ratio dielectric structures with high refractive index can generate waveguide modes, thus realizing a zero-order transmitted phase modulation with a high efficiency of more than 93%. It is challenging to obtain a similar result by using traditional platforms such as the ground glass or the spatial light modulator. Figure 2d shows the calculated information entropy with an increase of the disorder of the phase distribution. The information entropy is calculated by

$$H(\varphi) = -\sum_{j=1}^{N} p_j(\varphi)\log_N(p_j(\varphi)) \tag{6}$$

where N is the number to evenly segment the phase interval 0−2π, p_j (φ) is the possibility of the phase located in the j-th interval. The disordered phases result in different sizes of the instantaneous intensity speckles in the transmitted light (insets in Figure 2d), and larger information entropy corresponds to

https://doi.org/10.1021/acs.nanolett.2c02115
Nano Lett. 2022, 22, 6342−6349

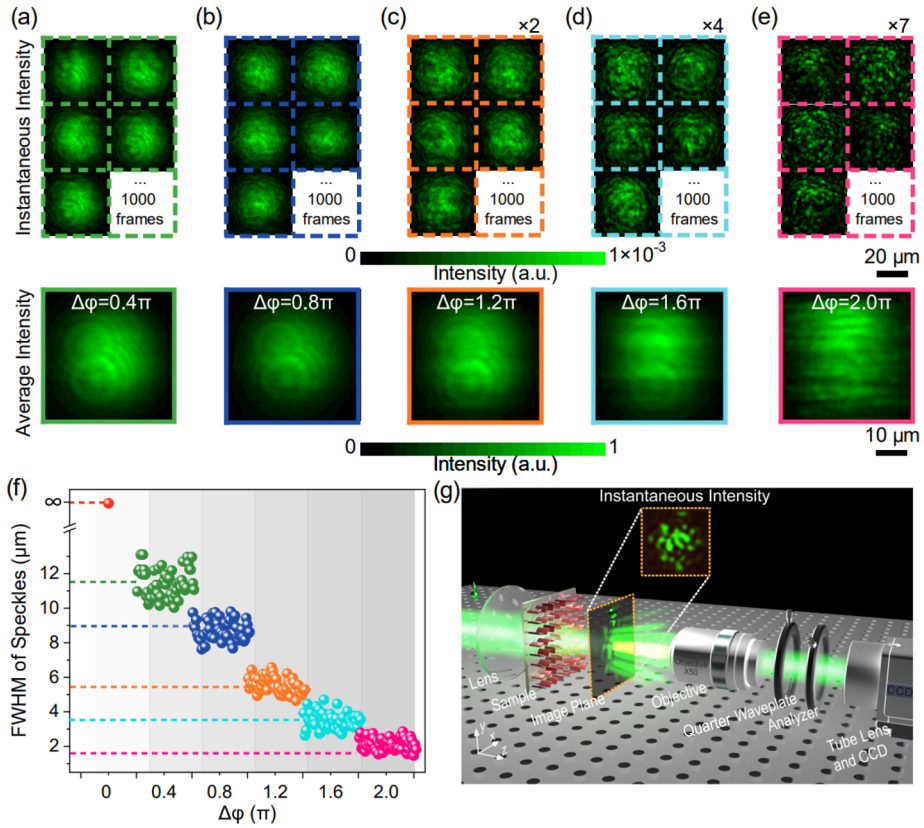

Figure 3. Measurement of the transmitted statistical speckles. (a–e) Experimental instantaneous intensity distributions (top) and corresponding average intensity of 1000 instantaneous intensities (bottom) for different PFRs. The intensities are normalized with the amendment coefficient on the top of (a–e). (f) Fluctuation of the measured fwhm of the speckles induced by the disordered arrangement of the nanofins. (g) Experimental setup to capture the instantaneous intensity distributions of the Gaussian-envelope beams. The statistical metasurface sample is located at $z = 0$ in the laboratory coordinate.

lower spatial coherence. The statistical metasurface can be easily fabricated using the standard atomic layer deposition method[35,36] through single-step lithography. The scanning electron micrograph of the fabricated sample is shown in Figure 2e. The total size of the fabricated statistical metasurface is 240 × 40 μm.

In the experiment, a left-handed circularly polarized Gaussian beam with a size of 30 μm was focused onto the statistical metasurface, which was a bit smaller than the width of the statistical metasurface to avoid information crosstalk. An electric translation stage controlled the movement of the statistical metasurface along the x-direction, loading a random phase change to the wavefront within a limited phase coverage. A cross-polarized imaging system was employed to capture 1000 instantaneous frames of speckles by unidirectionally scanning 240 μm for every coherence manipulation within 1 min, which is mainly limited by the time response of the charge-coupled device (CCD). There is no depolarization when the beam travel through the optical setup, and it is reasonable to use the scalar approach in our study (Figure S5). The lattice size of the metasurface is 330 nm, leading to incorporating the statistically scattering effects of new nanostructures in every frame. As a result, the normalized covariance of intensity fluctuations can be statistically considered "different" among different frames. The measured instantaneous intensities for different phase fluctuations show significant intensity speckles with the size related to the coherence length (Figure 3a–e). The defects in the light distribution can be attributed to fabrication imperfections. The average intensities are the MIF of the fluctuating EMWs at point $\mathbf{r} = \mathbf{r}_1 = \mathbf{r}_2$, which are calculated by averaging the 1000 instantaneous intensity distributions. The beamwidth w_0 of the generated speckled beams can be analyzed by adopting a theoretical Gaussian curve-fitting of the average intensity distributions. Figure 3f shows the fluctuation of the measured full width at half-maximum (fwhm) of the speckles for different PFRs, which apparently fluctuate in a limited range and decrease as the PFR increases. These fluctuations statistically determine the coherence properties of the transmitted beam. Each speckle can be viewed as a coherent superposition of the incident light, and the light emanating from the speckle should also be coherent.[37] In contrast, the light emanating from different light speckles is separated by different superposition processes, such as the low-intensity areas between the speckles arising due to the statistically averaged superposition. Thus, the size of the speckles can serve as a significant indicator of the coherence of the beam. The smaller the speckle, the lower the spatial coherence. Figure 3g illustrates the detailed experimental setup for capturing the aforementioned instantaneous intensity distributions shown in Figure 3a–e. Although in the prototype design we employed P–B phase to realize phase control, which additionally introduced waveplates and polarizers, the limitation is not fundamental. The major advantage of metaoptics is that by designing the local resonances, wavefront control can be efficiently realized and the polarized elements can be readily removed by using designs such as resonance-phase-based meta-atoms. In the experiments, we obtained the speckles distribution

https://doi.org/10.1021/acs.nanolett.2c02115
Nano Lett. 2022, 22, 6342–6349

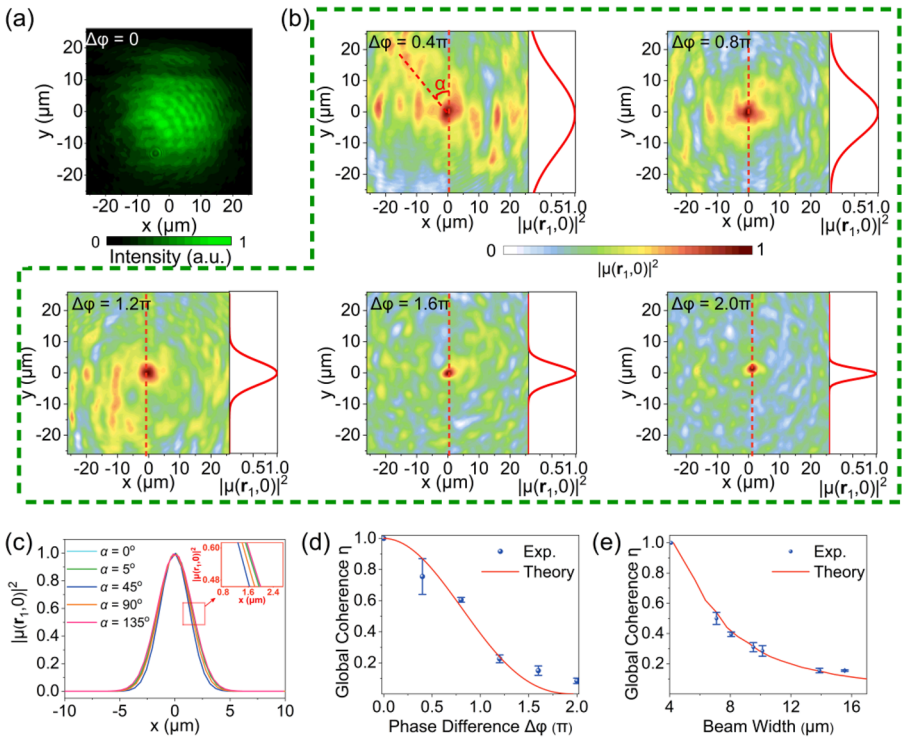

Figure 4. Spatial coherence manipulation based on the statistical metasurface. (a) Intensity profile of the fully coherent Gaussian beam at the $z = 120$ μm cut-plane. (b) Experimental distributions of $|\mu(\mathbf{r}_1, 0)|^2$ for different PFRs at the $z = 120$ μm cut-plane and the Gaussian curve-fitting along the $x = 0$ cut-line. The fwhms of the Gaussian curves indicate the coherence length of the generated partially coherent beams. (c) Gaussian curve-fitting of $|\mu(\mathbf{r}_1, 0)|^2$ for $\Delta\varphi = 2\pi$ for different cut-line orientation angles α, which is defined at the intersection with the $+y$ direction shown in (b). Inset: Zoom-in on the influence of α. (d,e) Comparison between the calculated and measured global DOC manipulated by (d) PFRs and (e) beamwidths. The error bar indicates the measured statistical fluctuation induced by the incomplete sets of cut-lines.

at $z = 120$ μm where the measured coherence had reached the convergence condition (see Supporting Information Sec. S4 and Figures S2−S4). Further details regarding the measurement can be found in Supporting Information Sec. S2.

Spatial coherence manipulation of the disorder-engineered statistical metasurfaces. The output light distributions captured by the CCD can be statistically analyzed to measure the normalized fourth-order correlation function (FOCF)[38]

$$g^{(2)}(\mathbf{r}_1, \mathbf{r}_2) = \frac{\frac{1}{M}\sum_{m=1}^{M} I^{(m)}(r_1) I^{(m)}(r_2)}{\overline{I}(r_1)\overline{I}(r_2)} \tag{7}$$

where $\overline{I}(\mathbf{r}_1)$ and $\overline{I}(\mathbf{r}_2)$ denote the averages of the captured instantaneous intensities at points $\mathbf{r}_1$ and $\mathbf{r}_2$. The probability distribution of the random phase embedded in the sample is spatially uniform, and the scanning speed of the process is timely uniform. The measured coherence can reach the convergence condition when the number of the captured frames is large enough. In the experiment, we captured $M = 1000$ pictures of the instantaneous intensity to achieve convergence of the normalized FOCF (Figure S6 shows the theoretical and experimental global coherence convergence for the different numbers of captured frames). On the other hand, the normalized FOCF is linearly dependent on the square of the modulus of the DOC function provided that the random process follows the Gaussian statistics, i.e.,

$$g^{(2)}(\mathbf{r}_1, \mathbf{r}_2) = 1 + |\mu(\mathbf{r}_1, \mathbf{r}_2)|^2 \tag{8}$$

Figure 4 further demonstrates the spatial coherence manipulation based on the disorder-engineered statistical metasurface. The intensity distribution of the fully coherent Gaussian beam is shown in Figure 4a. Figure 4b shows the experimental results of $|\mu(\mathbf{r}_1, \mathbf{r}_2 = 0)|^2$ for different PFRs. $|\mu(\mathbf{r}_1, \mathbf{r}_2 = 0)|^2$ is Gaussian-enveloped as the partially coherent beam belongs to the Gaussian Schell-Model. The coherence is irrelevant to the selected reference point.[39] The theoretical Gaussian curve-fittings were adopted to obtain the coherence length of the beams, as shown in Figure 4c. Although the Gaussian curve-fitting varies for different cut-line orientation angles, the calculated DOC is only affected by limited fluctuations for a specific PFR (Figure 4c and the inset). The Gaussian curve-fittings for different α values and PFRs are provided in Figure S7. We also calculated the global coherence $\eta = \delta_0/w_0$ for each PFR, where δ_0 denotes the coherence length of the output beam obtained via the theoretical fit, and w_0 denotes the beamwidth of the output beam in the experiments. Figure 4d,e shows the comparison between the theoretical and measured global coherence of the output light for different PFRs and the global coherence with different beam sizes for $\Delta\varphi = 2.0\pi$, respectively. It is noted that the lowest DOC is not approaching 0. Achieving a fully incoherent beam is a challenge, since it requires disordered wavefront manipulation with points of geometry size approaching infinitely small. Further experimental results regarding the intensity distributions and $|\mu(\mathbf{r}_1, \mathbf{r}_2 = 0)|^2$ for the spatial coherence manipulation with different beam sizes are provided in Figure S8.

Spatial coherence manipulation of other special beams. The proposed method can conveniently manipulate the spatial coherence of a wide range of special beams. Generally, the special beam can be realized through a transmission screen $T(x,$

https://doi.org/10.1021/acs.nanolett.2c02115
Nano Lett. 2022, 22, 6342−6349

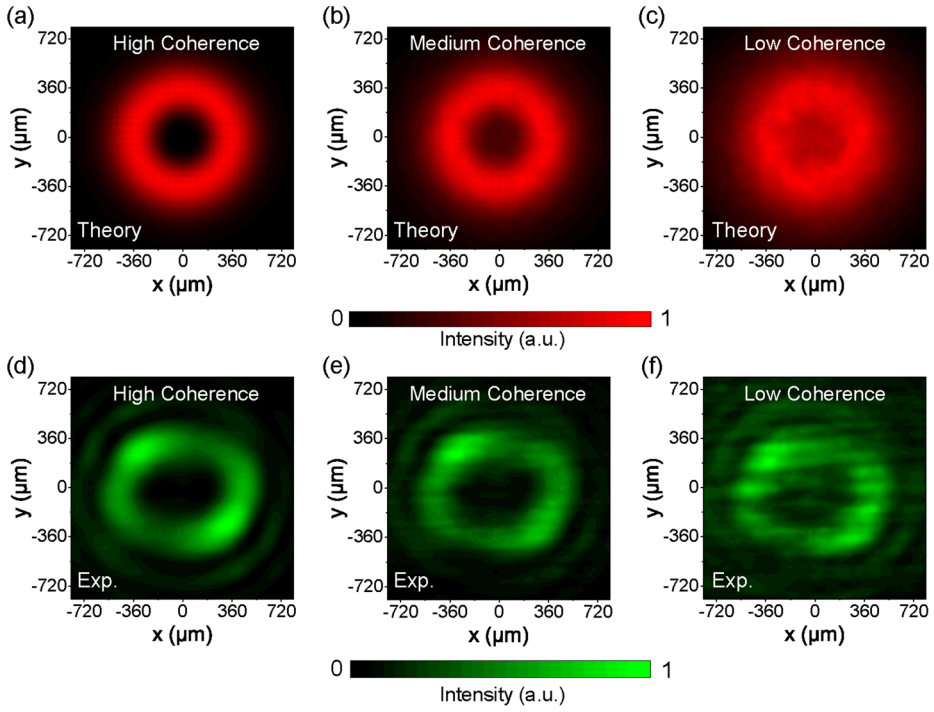

Figure 5. Spatial coherence manipulation of the vortex beams. (a−c) Theoretical calculations of the intensity distributions of the partially coherent vortex beams with different coherences. (d−f) Corresponding measured intensity distributions of the partially coherent vortex beams with different coherences. The central dark spot of the doughnut intensity profile for the partially coherent vortex beam becomes weaker with decreasing coherence due to the disordered phase distribution.

y) with specific amplitude and phase distributions. The complex envelope of the transmitted light is described as

$$A_t(x, y, t) = A_i(x, y, t - \tau_0)T(x, y) \tag{9}$$

where A_i is the complex envelope of the incident light, and τ_0 is the average time delay associated with the metasurface. Thus, the MIF of the transmitted light is given by

$$\Gamma_t(x_1, y_1; x_2, y_2) = \langle A_t(x_1, y_1, t)A_t^*(x_2, y_2, t)\rangle$$
$$= T(x_1, y_1)T^*(x_2, y_2)\langle A_t(x_1, y_1, t - \tau_0)A_t^*(x_2, y_2, t - \tau_0)\rangle \tag{10}$$

Accordingly, the general relationship between the incident and transmitted mutual intensity is

$$\Gamma_t(x_1, y_1; x_2, y_2) = T(x_1, y_1)T^*(x_2, y_2)\Gamma_i(x_1, y_1; x_2, y_2) \tag{11}$$

where Γ_i $(x_1, y_1; x_2, y_2)$ is the MIF of the incident light. Specifically, when T (x, y) is a unitary phase mask, the DOC of the transmitted beam is the same as that of the incident beam. Thus, we can load a unitary phase mask onto the generated partially coherent beam and obtain a special beam with the same spatial coherence. To demonstrate the spatial coherence manipulation of the special beams, we employed a vortex phase plate to modify the generated partially coherent beam (Figure 5). The calculated intensity distributions of the partially coherent vortex beams with different coherences are shown in Figure 5a−c, and the corresponding measurement is shown in Figure 5 d−f. The vortex phase plate incorporates an additional wavefront to the partially coherent beam generated by the statistical metasurface, which does not alter the beamwidth and spatial coherence. The central dark spot of the doughnut intensity profile for the partially coherent vortex beam phenomenologically becomes smaller and weaker with decreasing spatial coherence. Similar operations can also be applied to phase-only partially coherent hologram generation.

DISCUSSION

Compared with light fields with high coherence, partially coherent beams with lowered DOC can potentially improve the robustness of information transmission, especially when there are obstacles and artifacts in the optical path. It is worth noting that the limitation of phase-only based partially coherent special beam generation is not fundamental, and the transmission screen $T(x, y)$ with arbitrary amplitude and phase distribution can also be realized with proper metasurface design. Compared with conventional methods that control the spatial coherence of light by employing bulky disordered media, our approach significantly reduces the energy loss of the incident light, which further promotes the applications of partially coherent beams. Furthermore, it is also possible to achieve rapid modulation of the spatial coherence by adopting a microelectromechanical system[40] or employing structured light[41] to scan the sample. Based on the statistical metasurface for partially coherent beam generation, we envision robust information transmission in computational imaging[42] and wearable devices working in complex environment.[43]

In summary, we propose an extra-cavity-based strategy to accurately manipulate the spatial coherence of EMWs by loading a random phase distribution onto the wavefront on the statistical photonic platform. With highly efficient dielectric nanofins that can locally manipulate the correlation between different locations of EMWs, we realize the generation of partially coherent light with a predefined DOC and modulate the output beam from fully coherent to incoherent on the statistical metasurface platform. We also demonstrate the statistical

https://doi.org/10.1021/acs.nanolett.2c02115
Nano Lett. 2022, 22, 6342−6349

properties of the metasurface, such as information entropy, and apply this design strategy to generate partially coherent vortex beams, and the experimental results are consistent with the theory. This strategy not only significantly simplifies the experimental setups to generate partially coherent beams but also enables predesigned and accurate manipulation of the spatial coherence for different types of light beams. Our approach paves the way for further applications in information photonics such as turbulent information transmission and information retrieval in disordered or turbulent media.

■ ASSOCIATED CONTENT

Supporting Information

The Supporting Information is available free of charge at https://pubs.acs.org/doi/10.1021/acs.nanolett.2c02115.

Additional details on the sample fabrication, the measurement procedure, the design principle of the statistical metasurfaces, and the numerical simulation of the transmitted beam from the statistical metasurface (PDF)

Measured instantaneous intensity distributions for different PFRs while scanning (MP4)

■ AUTHOR INFORMATION

Corresponding Authors

Wenwei Liu − *The Key Laboratory of Weak Light Nonlinear Photonics, Ministry of Education, Renewable Energy Conversion and Storage Center, School of Physics and TEDA Institute of Applied Physics, Nankai University, Tianjin 300071, China*; Email: wliu@nankai.edu.cn

Hua Cheng − *The Key Laboratory of Weak Light Nonlinear Photonics, Ministry of Education, Renewable Energy Conversion and Storage Center, School of Physics and TEDA Institute of Applied Physics, Nankai University, Tianjin 300071, China*; Email: hcheng@nankai.edu.cn

Yangjian Cai − *Shandong Provincial Engineering and Technical Center of Light Manipulation & Shandong Provincial Key Laboratory of Optics and Photonic Device, School of Physics and Electronics, Shandong Normal University, Jinan 250014, China; School of Physical Science and Technology, Soochow University, Suzhou 215006, China*; Email: yangjiancai@suda.edu.cn

Shuqi Chen − *The Key Laboratory of Weak Light Nonlinear Photonics, Ministry of Education, Renewable Energy Conversion and Storage Center, School of Physics and TEDA Institute of Applied Physics, Nankai University, Tianjin 300071, China; The Collaborative Innovation Center of Extreme Optics, Shanxi University, Taiyuan, Shanxi 030006, China; The Collaborative Innovation Center of Light Manipulations and Applications, Shandong Normal University, Jinan 250358, China*; orcid.org/0000-0002-7898-4148; Email: schen@nankai.edu.cn

Authors

Leixin Liu − *Shandong Provincial Engineering and Technical Center of Light Manipulation & Shandong Provincial Key Laboratory of Optics and Photonic Device, School of Physics and Electronics, Shandong Normal University, Jinan 250014, China*

Fei Wang − *School of Physical Science and Technology, Soochow University, Suzhou 215006, China*

Duk-Yong Choi − *Laser Physics Centre, Research School of Physics, Australian National University, Canberra, ACT 2601, Australia*; orcid.org/0000-0002-5339-3085

Jianguo Tian − *The Key Laboratory of Weak Light Nonlinear Photonics, Ministry of Education, Renewable Energy Conversion and Storage Center, School of Physics and TEDA Institute of Applied Physics, Nankai University, Tianjin 300071, China*

Complete contact information is available at: https://pubs.acs.org/10.1021/acs.nanolett.2c02115

Notes

The authors declare no competing financial interest.

■ ACKNOWLEDGMENTS

This work was supported by the National Key Research and Development Program of China (2021YFA1400601 and 2019YFA0705000), the National Natural Science Fund for Distinguished Young Scholar (11925403), the National Natural Science Foundation of China (12122406, 12192253, 12192254, 11974193, 11974218, 11904183, and 11904181), the Natural Science Foundation of Tianjin for Distinguished Young Scientists (18JCJQJC45700), the China Postdoctoral Science Foundation (2021M690084), the Innovation Group of Jinan (2018GXRC010), and the Local Science and Technology Development Project of the Central Government (YDZX20203700001766). The metasurface nanofabrication was performed at the ACT node of the Australian National Fabrication Facility.

■ REFERENCES

(1) Zernike, F. The concept of degree of coherence and its application to optical problems. *Physica* **1938**, *5* (8), 785−795.

(2) Goodman, J. W. Coherence of optical Waves. In *Statistical Optics*, 2nd ed.; John Wiley & Sons, 2015; pp 157−226.

(3) Kato, Y.; Mima, K.; Miyanaga, N.; Arinaga, S.; Kitagawa, Y.; Nakatsuka, M.; Yamanaka, A. C. Random phasing of high-power lasers for uniform target acceleration and plasma-instability suppression. *Phys. Rev. Lett.* **1984**, *53* (11), 1057−1060.

(4) Paniagua-Diaz, A. M.; Starshynov, I.; Fayard, N.; Goetschy, A.; Pierrat, R.; Carminati, R.; Bertolotti, J. Blind ghost imaging. *Optica* **2019**, *6* (4), 460−464.

(5) Eliezer, Y.; Qu, G.; Yang, W.; Wang, Y.; Yılmaz, H.; Xiao, S.; Song, Q.; Cao, H. Suppressing meta-holographic artifacts by laser coherence tuning. *Light: Sci. Appl.* **2021**, *10* (1), 104.

(6) Deng, Y.; Wang, H.; Ji, X.; Li, X.; Yu, H.; Chen, L. Characteristics of high-power partially coherent laser beams propagating upwards in the turbulent atmosphere. *Opt. Express* **2020**, *28* (29), 27927−27939.

(7) Liu, M. J.; Chen, J.; Zhang, Y.; Shi, Y.; Zhao, C. L.; Jin, S. Z. Generation of coherence vortex by modulating the correlation structure of random lights. *Photonics Res.* **2019**, *7* (12), 1485−1492.

(8) Wang, J.; Chen, R.; Yao, J.; Ming, H.; Wang, A.; Zhan, Q. Random distributed feedback fiber laser generating cylindrical vector beams. *Phys. Rev. Appl.* **2019**, *11* (4), 044051.

(9) Leonetti, M.; Pattelli, L.; De Panfilis, S.; Wiersma, D. S.; Ruocco, G. Spatial coherence of light inside three-dimensional media. *Nat. Commun.* **2021**, *12* (1), 4199.

(10) Chen, X.; Li, J.; Rafsanjani, S. M. H.; Korotkova, O. Synthesis of Im-Bessel correlated beams via coherent modes. *Opt. Lett.* **2018**, *43* (15), 3590−3593.

(11) Wadood, S. A.; Liang, K.; Zhou, Y.; Yang, J.; Alonso, M. A.; Qian, X.-F.; Malhotra, T.; Hashemi Rafsanjani, S. M.; Jordan, A. N.; Boyd, R. W.; Vamivakas, A. N. Experimental demonstration of superresolution of partially coherent light sources using parity sorting. *Opt. Express* **2021**, *29* (14), 22034−22043.

(12) Knitter, S.; Liu, C.; Redding, B.; Khokha, M. K.; Choma, M. A.; Cao, H. Coherence switching of a degenerate VECSEL for multimodality imaging. *Optica* **2016**, *3* (4), 403−406.
(13) Cao, H.; Chriki, R.; Bittner, S.; Friesem, A. A.; Davidson, N. Complex lasers with controllable coherence. *Nat. Rev. Phys.* **2019**, *1* (2), 156.
(14) Vanneste, C.; Sebbah, P.; Cao, H. Lasing with resonant feedback in weakly scattering random systems. *Phys. Rev. Lett.* **2007**, *98* (14), 143902.
(15) Mahler, S.; Eliezer, Y.; Yılmaz, H.; Friesem, A. A.; Davidson, N.; Cao, H. Fast laser speckle suppression with an intracavity diffuser. *Nanophotonics* **2020**, *10* (1), 129−136.
(16) Koivurova, M.; Hakala, T. K.; Turunen, J.; Friberg, A. T.; Caglayan, H.; Ornigotti, M. Coherence Switching with Metamaterials. *Phys. Rev. Lett.* **2021**, *127* (15), 153902.
(17) Hyde, M. W.; Bose-Pillai, S.; Voelz, D. G.; Xiao, X. Generation of Vector Partially Coherent Optical Sources Using Phase-Only Spatial Light Modulators. *Phys. Rev. Appl.* **2016**, *6* (6), 064030.
(18) Gao, Y. J.; Xiong, X.; Wang, Z.; Chen, F.; Peng, R. W.; Wang, M. Simultaneous generation of arbitrary assembly of polarization states with geometrical-scaling-induced phase modulation. *Phys. Rev. X* **2020**, *10* (3), 031035.
(19) Liu, W.; Li, Z.; Cheng, H.; Tang, C.; Li, J.; Zhang, S.; Chen, S.; Tian, J. Metasurface enabled wide-angle Fourier Lens. *Adv. Mater.* **2018**, *30* (23), 1706368.
(20) Manjappa, M.; Pitchappa, P.; Singh, N.; Wang, N.; Zheludev, N. I.; Lee, C.; Singh, R. Reconfigurable MEMS Fano metasurfaces with multiple-input-output states for logic operations at terahertz frequencies. *Nat. Commun.* **2018**, *9* (1), 4056.
(21) Koshelev, K.; Kruk, S.; Melik-Gaykazyan, E.; Choi, J. H.; Bogdanov, A.; Park, H. G.; Kivshar, Y. Subwavelength dielectric resonators for nonlinear nanophotonics. *Science* **2020**, *367* (6475), 288−292.
(22) Hu, G.; Hong, X.; Wang, K.; Wu, J.; Xu, H. X.; Zhao, W.; Liu, W.; Zhang, S.; Garcia-Vidal, F.; Wang, B.; Lu, P. X.; Qiu, C. W. Coherent steering of nonlinear chiral valley photons with a synthetic au-ws2 metasurface. *Nat. Photonics* **2019**, *13* (7), 467.
(23) Yoda, T.; Notomi, M. Generation and annihilation of topologically protected bound states in the continuum and circularly polarized states by symmetry breaking. *Phys. Rev. Lett.* **2020**, *125* (5), 053902.
(24) Yuan, Y.; Sun, S.; Chen, Y.; Zhang, K.; Ding, X.; Ratni, B.; Wu, Q.; Burokur, S. N.; Qiu, C. W. A fully phase-modulated metasurface as an energy-controllable circular polarization router. *Adv. Sci.* **2020**, *7* (18), 2001437.
(25) Dorrah, A. H.; Rubin, N. A.; Zaidi, A.; Tamagnone, M.; Capasso, F. Metasurface optics for on-demand polarization transformations along the optical path. *Nat. Photonics* **2021**, *15* (4), 287.
(26) Picardi, M. F.; Zayats, A. V.; Rodríguez-Fortuño, F. J. Janus and Huygens dipoles: near-field directionality beyond spin-momentum locking. *Phys. Rev. Lett.* **2018**, *120* (11), 117402.
(27) Kruk, S.; Hopkins, B.; Kravchenko, I. I.; Miroshnichenko, A.; Neshev, D. N.; Kivshar, Y. S. Invited Article: Broadband highly efficient dielectric metadevices for polarization control. *APL Photonics* **2016**, *1* (3), 030801.
(28) Fan, Q.; Liu, M.; Zhang, C.; Zhu, W.; Wang, Y.; Lin, P.; Yan, F.; Chen, L.; Lezec, H. J.; Lu, Y.; Agrawal, A.; Xu, T. Independent amplitude control of arbitrary orthogonal states of polarization via dielectric metasurfaces. *Phys. Rev. Lett.* **2020**, *125* (26), 267402.
(29) Arbabi, A.; Horie, Y.; Bagheri, M.; Faraon, A. Dielectric metasurfaces for complete control of phase and polarization with subwavelength spatial resolution and high transmission. *Nat. Nanotechnol.* **2015**, *10* (11), 937−943.
(30) Devlin, R. C.; Ambrosio, A.; Rubin, N. A.; Mueller, J. B.; Capasso, F. Arbitrary spin-to-orbital angular momentum conversion of light. *Science* **2017**, *358* (6365), 896−901.
(31) Chen, S.; Li, Z.; Liu, W.; Cheng, H.; Tian, J. From single-dimensional to multidimensional manipulation of optical waves with metasurfaces. *Adv. Mater.* **2019**, *31* (16), 1802458.
(32) Li, D.; Pacifici, D. Strong amplitude and phase modulation of optical spatial coherence with surface plasmon polaritons. *Sci. Adv.* **2017**, *3* (10), 1700133.
(33) Wolf, E. Second-order coherence phenomena in the space-time domain. In *Introduction to the Theory of Coherence and Polarization of Light*; Cambridge Univ. Press, 2007; pp 31−37.
(34) Eichmann, U.; Bergquist, J. C.; Bollinger, J. J.; Gilligan, J. M.; Itano, W. M.; Wineland, D. J.; Raizen, M. G. Young's interference experiment with light scattered from two atoms. *Phys. Rev. Lett.* **1993**, *70* (16), 2359.
(35) Khorasaninejad, M.; Capasso, F. Metalenses: Versatile multifunctional photonic components. *Science* **2017**, *358* (6367), No. eaam8100.
(36) Liu, W.; Ma, D.; Li, Z.; Cheng, H.; Choi, D. Y.; Tian, J.; Chen, S. Aberration-corrected three-dimensional positioning with a single-shot metalens array. *Optica* **2020**, *7* (12), 1706−1713.
(37) Magatti, D.; Gatti, A.; Ferri, F. Three-dimensional coherence of light speckles: Experiment. *Phys. Rev. A* **2009**, *79* (5), 053831.
(38) Wang, F.; Cai, Y. Experimental observation of fractional Fourier transform for a partially coherent optical beam with Gaussian statistics. *J. Opt. Soc. Am. A* **2007**, *24* (7), 1937−1944.
(39) Friberg, A. T.; Sudol, R. J. Propagation parameters of Gaussian Schell-model beams. *Opt. Commun.* **1982**, *41* (6), 383−387.
(40) Arbabi, E.; Arbabi, A.; Kamali, S. M.; Horie, Y.; Faraji-Dana, M.; Faraon, A. MEMS-tunable dielectric metasurface lens. *Nat. Commun.* **2018**, *9* (1), 812.
(41) Forbes, A.; de Oliveira, M.; Dennis, M. R. Structured light. *Nat. Photonics* **2021**, *15* (4), 253−262.
(42) Luo, Y.; Zhao, Y.; Li, J.; Çetintaş, E.; Rivenson, Y.; Jarrahi, M.; Ozcan, A. Computational imaging without a computer: seeing through random diffusers at the speed of light. *eLight* **2022**, *2*, 4.
(43) Ma, Q.; Gao, W.; Xiao, Q.; Ding, L.; Gao, T.; Zhou, Y.; Gao, X.; Yan, T.; Liu, C.; Gu, Z.; Kong, X.; Abbasi, Q. H.; Li, L.; Qiu, C. W.; Li, Y.; Cui, T. J. Directly wireless communication of human minds via non-invasive brain-computer-metasurface platform. *eLight* **2022**, *2*, 11.

https://doi.org/10.1021/acs.nanolett.2c02115
Nano Lett. 2022, 22, 6342−6349